Equations of state for B2 and bcc $Fe_{1-x}Si_x$

Yoshihiro Nagaya[1,*], Hitoshi Gomi[2,3,*], Kenji Ohta[1], and Kei Hirose[2,3]

[1]Department of Earth and Planetary Sciences, Tokyo Institute of Technology, Tokyo, Japan
[2]Department of Earth and Planetary Science, The University of Tokyo, Tokyo, Japan
[3]Earth-Life Science Institute, Tokyo Institute of Technology, Tokyo, Japan

* Corresponding authors. E-mail addresses: nagaya.y.ab@m.titech.ac.jp, hitoshi.gomi@eps.s.u-tokyo.ac.jp

Abstract

Composition, chemical disorder, and magnetism significantly affect the volume and bulk modulus of iron–silicon (Fe–Si) alloys at ambient pressure. Here, we computed the equations of state for bcc-like (ordered B2 and disordered bcc) Fe–Si alloys available up to the inner-core pressure using the first-principles Korringa–Kohn–Rostoker method. Ferromagnetic (FM) and nonmagnetic (NM) states over a wide composition range, from Fe to FeSi, were investigated. The results revealed that magnetism and chemical disorder increased the volume and decreased the bulk modulus even at high pressures. Comparing the results with the preliminary reference Earth model, we found that an unrealistically large temperature gradient is required if the inner core is composed of a bcc-like Fe–Si alloy.

Plain Language Summary

The center of the Earth is composed of a massive iron sphere known as the inner core, with a radius of 1221 km. This inner core is subjected to high pressure (>330 GPa) and temperature (approximately 5000 K). Under these extreme conditions, the density and sound-wave propagation speed are very different from those of the materials on Earth's surface. Key unsolved problems pertaining to the inner core are its chemical composition and crystal structure. To resolve this issue, computer simulations were performed to determine the density and sound speed of Fe–Si alloys under temperature and pressure conditions corresponding to the inner core. We investigated various parameters of Fe–Si alloys while maintaining a crystal structure similar to that of iron under ambient conditions. These parameters included the iron-to-silicon ratio, strength of the magnetism of iron atoms, and the degree of ordering of atomic positions. These parameters affected the density and sound speed; however, we found that no combination of the parameters satisfied the seismic observations throughout the inner core. Therefore, the inner core may have a different crystal structure or contain impurities other than silicon.

Key Points:

- We conducted first-principles calculations to obtain the equations of state for B2 and body-centered-cubic Fe–Si alloys.

- The presence of magnetism and chemical disorder increased the volume and decreased the bulk modulus of the examined Fe–Si alloys.
- Single-phase bcc-like $Fe_{1-x}Si_x$ cannot satisfy the seismic observation of the Earth's inner core.

1. Introduction

Earth's inner core is thought to be composed of an iron alloy containing nickel and a small percentage of light elements (Birch, 1952; Hirose et al., 2021). Silicon is one of the most likely candidates for the hypothesized light elements. A large amount of silicon may have been incorporated into core-forming metals, particularly under reducing conditions, to form Fe–Si alloys (McDonough et al., 2003; Ricolleau et al., 2011). Comparisons of the Mg/Si and Fe/Si ratios between Earth's mantle and chondrites also indicate a possibility of silicon enrichment in the core (Allegre et al., 1995). If silicon is the major light element in the inner core, in addition to the aforementioned geochemical constraints, the density and elastic wave velocity of Fe–Si alloys should match seismic observations (Mao et al., 2012; Sakamaki et al., 2016; Shibazaki et al., 2016).

The crystal structure strongly influences the density and elastic-wave velocity of metals. Previous diamond anvil cell experiments have suggested that the stable structure of pure iron is a hexagonal close-packed (hcp) structure under the temperature and pressure conditions of the inner core (Tateno et al., 2010; Sakai et al., 2011). However, previous first-principles studies proposed two conflicting crystal structures: the hcp structure (Stixrude & Cohen, 1995), and the body-centered cubic (bcc) structure (Niu et al., 2015; Belonoshko et al., 2017). Furthermore, the bcc structure can be stabilized by adding small amounts of impurities to iron (Vočadlo et al., 2003; Kádas et al., 2009). Silicon is a bcc-stabilizer as Fe–Si alloys adopt bcc and bcc-like structures such as B2 (Fischer et al., 2013; Tateno et al., 2015; Ozawa et al., 2016; Edmund et al., 2019, 2022; Ikuta et al., 2021; Fu et al., 2022). B2 FeSi is an ordered phase; iron and silicon atoms occupy the (0 0 0) and (1/2 1/2 1/2) sites, respectively (Figure S1a). In contrast, bcc Fe–Si is a disordered phase in which the two atoms are randomly aligned (Figure S1b). In this study, we focused on bcc and B2 Fe_{1-}

$_xSi_x$.

In addition to crystal structure, magnetism also affects the density and elastic-wave velocity. Several researchers have investigated the relationship between magnetism and the physical properties of bcc-like (bcc, B2, and DO_3) $Fe_{1-x}Si_x$ at ambient pressures (Elsukov et al., 1992; Kudrnovský et al., 1991; Kulikov et al., 2002). Elsukov et al. (1992) performed Mössbauer measurements on disordered crystalline and amorphous $Fe_{1-x}Si_x$ alloys with variable silicon concentrations. Kudrnovský et al. (1991) performed first-principles calculations for DO_3 $Fe_{3+x}Si_{1-x}$ with partial disordering using the linear muffin-tin orbital method combined with the coherent potential approximation (CPA) with fixed lattice parameters. These two studies (Elsukov et al., 1992; Kudrnovský et al., 1991) showed that the local magnetic moment of iron increases as the number of nearest-neighbor (NN) iron atoms increases (Kulikov et al., 2002). Kulikov et al. (2002) used the Korringa–Kohn–Rostoker (KKR) method in combination with CPA to calculate bcc $Fe_{1-x}Si_x$ with varying lattice parameters. Their results demonstrated that the magnetic moment decreases with increasing silicon concentrations, which causes a decrease in volume and an increase in the bulk modulus. In summary, the magnetic moment varies with the number of NN iron atoms, which is determined by the composition and chemical disorder, resulting in a volume increase and a decrease in the bulk modulus.

In this study, we computed the equations of state (EoS) for $Fe_{1-x}Si_x$ under pressure conditions matching the Earth's inner core based on the KKR-CPA method (with and without considering magnetism), regardless of its thermodynamic stability. We considered the bcc and B2 structures, which maximize and minimize the number of NN iron atoms, respectively. Using the present EoS, we calculated the density and bulk sound velocity of $Fe_{1-x}Si_x$ alloys and compared them with the inner-core observations provided by the Preliminary Reference Earth Model (PREM) (Dziewonski & Anderson, 1981).

2. Methods

We obtained the equations of state of the $Fe_{1-x}Si_x$ alloys (x = 0, 0.1, 0.2, 0.3, 0.4, and

0.5) based on static first-principles calculations. Figure S1a shows the crystal structure of fully ordered B2 FeSi (x = 0.5). Figure S1b shows the bcc FeSi, in which the number of NN iron atoms and the degree of disordering are maximized. For non-stoichiometric compositions ($0 < x < 0.5$), the structure with the highest degree of ordering was B2, and the lowest was bcc. In the fully ordered B2 structure, the Fe sites were completely occupied by iron atoms, whereas Si sites were occupied by both iron and silicon atoms. Figure S1c shows the most ordered structure of the B2 $Fe_{0.6}Si_{0.4}$. In this structure, iron atoms occupy all the (0 0 0) sites (Fe sites) and 20% of the (1/2 1/2 1/2) sites (Si sites). On the other hand, Fe and Si sites were not distinguished; thus, iron and silicon atoms were randomly positioned in the bcc structure (Figures S1a, d). In this study, we considered the structures with the highest and lowest degrees of ordering among the B2 and bcc structures.

The Kohn–Sham equation (Kohn & Sham, 1965) was solved using the KKR method (Akai, 1989). We used the CPA to simulate chemical disorder. We considered the ferromagnetic (FM) and non-magnetic (NM) states, which can be obtained by spin-polarized and non-spin-polarized calculations. The volume range was 75–200 $Bohr^3$ (11.11–29.64 $Å^3$). The Perdew–Burke–Ernzerhof (PBE) type of generalized gradient approximation (GGA) was used as the exchange-correlation functional (Perdew et al., 1996). We treated relativistic effects within the scalar relativistic approximation. We calculated the wavefunction up to l = 2, where l is the angular momentum quantum number. This method has been used for the FeH_x system, with results consistent with those of previous experiments (Gomi et al., 2018; Tagawa et al., 2022; Gomi & Hirose, 2022). We used a simple cubic lattice for a computational cell containing two atoms for all calculations. A k-point mesh of 20 × 20 × 20 was used, corresponding to 1771 points in the irreducible Brillouin zone.

The total energy was fitted to the third-order Birch–Murnaghan equation of state:

$$E(V) = \frac{9V_0K_{T,0}}{16}\left\{\left[\left(\frac{V_0}{V}\right)^{\frac{2}{3}} - 1\right]^3 K' + \left[\left(\frac{V_0}{V}\right)^{\frac{2}{3}} - 1\right]^2 \left[6 - 4\left(\frac{V_0}{V}\right)^{\frac{2}{3}}\right]\right\} + E_0 \quad (1)$$

where E is the total energy, V is the volume, K_T is the isothermal bulk modulus, and K' is the pressure derivative. The subscript '0' refers to the value at zero pressure. In the

spin-polarized calculations, we fitted the volume range in which the local magnetic moment of the iron atom in the Fe site exists. The pressure $P = -dE/dV$ and isothermal bulk modulus $K_T = V(d^2E/dV^2)_T$ were obtained from the analytical derivative.

3. Results

Figure 1 shows the results of the present equations of state for $Fe_{1-x}Si_x$ compared with those of previous experiments (Dewaele et al., 2006; Edmund et al., 2019; Sata et al., 2010). The fitting parameters are summarized in Table S1-4. The magnetic moment (M_0), volume (V_0), and isothermal bulk modulus ($K_{T,0}$) were plotted at ambient pressure (Figure 2). The combination of the crystal structure (B2 and bcc) and magnetism (FM and NM) significantly changed these quantities.

Figure 1a shows FM B2 $Fe_{1-x}Si_x$, which best explains the previous experiments (Dewaele et al., 2006; Edmund et al., 2019; Sata et al., 2010) for the combination of magnetism and crystal structure investigated in this study. The volume was largest for pure iron and decreased with increasing silicon concentrations (Figure 2b). This volume change is related to the bulk magnetic moment (Kulikov et al., 2002). The bulk magnetic moment at 0 GPa decreases with increasing silicon concentrations and becomes zero for FeSi (Figure 2a). This is consistent with previous Mössbauer measurements (Elsukov et al., 1992) and first-principles calculations (Kudrnovský et al., 1991; Kulikov et al., 2002).

Figure 1b compares the NM B2 $Fe_{1-x}Si_x$ with previous experiments. Except for FeSi ($x = 0.5$), where spin-polarized calculations yielded NM results, the volume of NM was smaller than those calculated in previous experiments (Dewaele et al., 2006; Edmund et al., 2019). This indicates the importance of magnetism in the equations of state for $Fe_{1-x}Si_x$.

Figure 1c illustrates FM bcc $Fe_{1-x}Si_x$. Pure iron was reproduced in a previous experiment (Dewaele et al., 2006). However, the difference between the present calculation and previous experiments (Edmund et al., 2019; Sata et al., 2010) increased with increasing silicon concentrations. Ferromagnetic bcc $Fe_{1-x}Si_x$ also showed a decreasing bulk magnetic moment with increasing silicon concentrations, similar to

FM B2. However, at the maximum silicon concentration of FeSi (x = 0.5), B2 FeSi became NM, whereas bcc FeSi remained FM. This difference in the compositional dependence of the magnetic moment between B2 and bcc is consistent with previous studies at 1 bar (Khmelevska et al., 2006; Rinaldi et al., 2021). This behavior can be understood within the model, which suggests that the magnetic moment is proportional to the number of NN iron atoms (Elsukov et al., 1992; Kudrnovský et al., 1991); all bonds in B2 FeSi are Fe-Si, whereas 25% of the bonds in bcc FeSi are Fe-Fe.

Figure 1d shows the volume of NM bcc $Fe_{1-x}Si_x$ as a function of the pressure. The iron volume was underestimated because of the absence of magnetism. Interestingly, the equation of state of NM bcc FeSi differs from that of NM B2 FeSi. In the above discussion, the relationship between the chemical disorder and volume was interpreted as the effect of magnetism. However, the NM bcc $Fe_{1-x}Si_x$ results suggest that chemical disorder also affects the volume and bulk modulus.

4. Discussion

The volume and bulk modulus are crucial in the examination of bcc-like $Fe_{1-x}Si_x$ alloys as a predominant mineral in the inner core based on comparing their densities and bulk sound velocities with seismic observations. Our important findings are as follows: 1) The magnetic moment depends on the number of NN iron atoms, which changes with silicon concentration and chemical disorder; 2) The higher the magnetic moment, the larger the volume, and the smaller the bulk modulus; 3) Without considering magnetism, the bcc alloy has a larger volume and lower bulk modulus than the B2 alloy.

While these findings are consistent with those of previous studies at ambient pressure (Elsukov et al., 1992; Kudrnovský et al., 1991; Kulikov et al., 2002), they are not consistent with the earlier high-pressure/room-temperature experiments performed by Edmund et al. (2018), which identified the $Fe_{1-x}Si_x$ samples with $x > 0.21$ to be in the metastable bcc phase. In contrast, our calculations for bcc $Fe_{1-x}Si_x$ did not reproduce their equations of state (Figures 1c and 1d). There are two possibilities that may explain this discrepancy. First, Edmund et al. (2018) misidentified the B2 and DO_3

structures as bcc. Body-centered cubic phase identification was based on the absence of the diffraction line, which is characteristic of the ordered phase. However, the intensity of this characteristic B2 line was weak and difficult to observe. Another possibility is that the present calculations overestimated the effects of FM. In general, GGA tends to overestimate the volume and magnetic moment. Indeed, the magnetic moment obtained in this study was higher than that reported in the literature (Figure 2a). Furthermore, at finite temperatures, the bulk magnetic moment decreases owing to the spin fluctuations.

The finite temperature effect on the magnetic disorder in magnetic phases becomes more critical at the high temperatures corresponding to the inner core. The same is true for the chemical disorder in the B2 phase. It is highly challenging to optimize the thermodynamic properties of the chemical and magnetic order parameters, which may vary continuously at finite temperatures. Alternatively, this study considers four different combinations of crystal structure (B2 or bcc) and magnetism (FM or NM) as end components to discuss the inner-core density and bulk sound velocity.

5. Implications

Figure 3 shows the density and bulk sound velocity as functions of pressure at 0 K for B2 and bcc $Fe_{1-x}Si_x$. For FM, we plotted data only within the pressure range where spin-polarized calculations provided a finite magnetic moment at the Fe site. In the case of pure iron, it is possible to have local magnetic moments up to the inner-core pressures. For bcc $Fe_{1-x}Si_x$, the pressure range with finite magnetic moments became narrower as the silicon concentration increased. However, this pressure range becomes wider for B2 $Fe_{1-x}Si_x$ than for bcc. Ferromagnetic material has a lower density and slower bulk sound velocity than NM. However, these differences were smaller at higher pressures. For all calculations, with increasing silicon concentrations, the density decreased, and the bulk sound velocity increased. This finding is consistent with those of Hirao et al. (2004) and Fischer et al. (2014).

For $Fe_{1-x}Si_x$ to be the sole constituent of the inner core, its density and bulk sound velocity must be consistent with the seismic observations. Ferromagnetic and NM iron

have higher densities and slower bulk sound velocities than PREM values (Dziewonski & Anderson, 1981) at the inner-core-boundary (ICB) pressure and 0 K (Figure 4a). Alloying silicon causes a decrease in density and an increase in bulk sound velocity. At 0 K, both the density and bulk sound volume of NM $Fe_{1-x}Si_x$ do not match the PREM simultaneously at any silicon concentration. In contrast, FM bcc $Fe_{1-x}Si_x$ with $x \sim 0.15$ is closely consistent with the PREM. If the inner-core temperature is 0 K, NM $Fe_{1-x}Si_x$ is no longer a candidate for the inner core, whereas FM bcc $Fe_{0.85}Si_{0.15}$ is a strong candidate. However, the inner core is in a high-temperature state (T ~5000 K), which reduces the density and bulk sound velocity. Therefore, we need to examine the effects of temperature on NM $Fe_{1-x}Si_x$.

We calculated the Helmholtz energies of NM B2 and bcc $Fe_{1-x}Si_x$ under inner-core conditions following Gomi and Hirose (2022). The contributions of the electrons were determined based on the density of states (DOS) of the system. The lattice vibration terms were examined using a quasi-harmonic approximation with the Debye model. To obtain the Debye temperature, we assumed that the Poisson's ratio of $Fe_{1-x}Si_x$ was identical to the PREM value; note that this assumption is valid when the inner core consists of $Fe_{1-x}Si_x$. Under this assumption, the high-temperature density and bulk sound velocity of bcc-like NM $Fe_{1-x}Si_x$ at ICB pressure and T = 0 K and 5000 K are compared with those of PREM in Figure 4b. We found that NM B2 $Fe_{1-x}Si_x$ (x = 0.074) explained both the PREM density and bulk sound velocity at T = 4820 K. With such a low silicon concentration, the values for bcc were similar to those for B2 at any depth of the inner core. Figure 5 shows the variations in the silicon content and temperature for NM bcc-like $Fe_{1-x}Si_x$ to simultaneously satisfy the PREM density and bulk sound velocity as a function of the radial position inside the inner core. This indicates that large gradients in both silicon concentration and temperature are required. However, if this is the case, the temperature difference between the ICB and the center of the Earth is 2300 K. For thermal stratification, the temperature gradient must be smaller than the adiabatic temperature gradient. However, ΔT = 2300 K is much greater than the temperature difference of ~200 K along the adiabatic temperature gradient (Figure 5b) that is expressed as $T(r) = T_{ICB}(\rho(r)/\rho_{ICB})^{\gamma}$, where r is radial position in the inner core, ρ is density, and γ = 1.45 is the Grüneisen parameter for B2 $Fe_{1-x}Si_x$ at ICB conditions

(Equation S17). Therefore, the thermal stratification required for the B2 Fe–Si alloy to be the inner-core material is not feasible. The effect of magnetism is weaker at higher temperatures and pressures toward the center of the inner core, which further increases the temperature gradient required. Therefore, the bcc-like $Fe_{1-x}Si_x$ binary alloy did not explain the seismic observations of the inner core. Indeed, the eutectic liquid composition in the Fe–FeSi system was estimated to be Fe + 8 wt.% Si ($Fe_{0.85}Si_{0.15}$) at 330 GPa (Hasegawa et al., 2021), suggesting that B2 Fe–Si alloy contains silicon volumes that exceed the eutectic composition (>15 at.% Si) under inner-core conditions. Since only 3–7 at.% silicon is required to explain the inner-core seismic observations (Figure 5b), Si-rich B2 Fe–Si cannot be the predominant constituent of the inner core.

Acknowledgments

This work was supported by JSPS MEXT/KAKENHI Grants 20K22365 and 22K03754. We would like to thank Editage (www.editage.com) for English language editing.

Open Research

Datasets for this research are found in Table S1, S2, S3, and S4 available online (https://doi.org/10.5281/zenodo.7483988)

References

Akai, H. (1989). Fast Korringa-Kohn-Rostoker coherent potential approximation and its application to FCC Ni-Fe systems. *Journal of Physics: Condensed Matter,* 1(43), 8045. https://doi.org/10.1088/0953-8984/1/43/006

Allegre, C. J., Poirier, J. P., Humler, E., & Hofmann, A. W. (1995). The chemical composition of the Earth. *Earth and Planetary Science Letters*, *134*(3-4), 515-526. https://doi.org/10.1016/0012-821X(95)00123-T

Belonoshko, A. B., Lukinov, T., Fu, J., Zhao, J., Davis, S., & Simak, S. I. (2017). Stabilization of body-centred cubic iron under inner-core conditions. *Nature Geoscience*, 10(4), 312-316. https://doi.org/10.1038/ngeo2892

Birch, F. (1952). Elasticity and constitution of the Earth's interior. *Journal of Geophysical Research*, 57(2), 227-286. https://doi.org/10.1029/JZ057i002p00227

Dewaele, A., Loubeyre, P., Occelli, F., Mezouar, M., Dorogokupets, P. I., & Torrent, M. (2006). Quasihydrostatic equation of state of iron above 2 Mbar. *Physical Review Letters*, *97*(21), 215504. https://doi.org/10.1103/PhysRevLett.97.215504

Dziewonski, A. M., & Anderson, D. L. (1981). Preliminary reference Earth model. *Physics of the Earth and Planetary Interiors*, 25(4), 297-356. https://doi.org/10.1016/0031-9201(81)90046-7

Edmund, E., Antonangeli, D., Decremps, F., Morard, G., Ayrinhac, S., Gauthier, M., Boulard, E., Mezouar, M.,, Hanfland, M., & Guignot, N. (2019). Structure and elasticity of cubic Fe-Si alloys at high pressures. *Physical Review B*, *100*(13), 134105. https://doi.org/10.1103/PhysRevB.100.134105

Edmund, E., Morard, G., Baron, M. A., Rivoldini, A., Yokoo, S., Boccato, S., Hirose, K., Pakhomova, A., & Antonangeli, D. (2022). The Fe-FeSi phase diagram at Mercury's core conditions. *Nature Communications*, 13(1), 1-9. https://doi.org/10.1038/s41467-022-27991-9

Elsukov, E. P., Konygin, G. N., Barinov, V. A., & Voronina, E. V. (1992). Local atomic environment parameters and magnetic properties of disordered crystalline and amorphous iron-silicon alloys. *Journal of Physics: Condensed Matter*, 4(37), 7597. https://doi.org/10.1088/0953-8984/4/37/007

Fischer, R. A., Campbell, A. J., Caracas, R., Reaman, D. M., Heinz, D. L., Dera, P., & Prakapenka, V. B. (2014). Equations of state in the Fe - FeSi system at high pressures and temperatures. *Journal of Geophysical Research: Solid Earth*, *119*(4), 2810-2827. https://doi.org/10.1002/2013JB010898

Fischer, R. A., Campbell, A. J., Reaman, D. M., Miller, N. A., Heinz, D. L., Dera, P., & Prakapenka, V. B. (2013). Phase relations in the Fe–FeSi system at high pressures and temperatures. *Earth and Planetary Science Letters*, 373, 54-64. https://doi.org/10.1016/j.epsl.2013.04.035

Fu, S., Chariton, S., Prakapenka, V. B., Chizmeshya, A., & Shim, S. H. (2022). Stable hexagonal ternary alloy phase in Fe-Si-H at 28.6–42.2 GPa and 3000 K. *Physical Review B*, *105*(10), 104111. https://doi.org/10.1103/PhysRevB.105.104111

Gomi, H., Fei, Y., & Yoshino, T. (2018). The effects of ferromagnetism and interstitial hydrogen on the equation of states of hcp and dhcp FeH_x: Implications for the Earth's inner core age. *American Mineralogist: Journal of Earth and Planetary Materials*, 103(8), 1271-1281. https://doi.org/10.2138/am-2018-6295

Gomi, H., & Hirose, K., (in press). Magnetism and equation of states of fcc FeH_x at high pressure. *American Mineralogist: Journal of Earth and Planetary Materials*, https://doi.org/10.2138/am-2022-8452

Hasegawa, M., Hirose, K., Oka, K., & Ohishi, Y. (2021). Liquidus phase relations and solid-liquid partitioning in the Fe-Si-C system under core pressures. *Geophysical Research Letters*, 48(13), e2021GL092681. https://doi.org/10.1029/2021GL092681

Hirao, N., Ohtani, E., Kondo, T., & Kikegawa, T. (2004). Equation of state of iron–silicon alloys to megabar pressure. *Physics and Chemistry of Minerals*, 31(6), 329-336. https://doi.org/10.1007/s00269-004-0387-x

Hirose, K., Wood, B., & Vočadlo, L. (2021). Light elements in the Earth's core. *Nature Reviews Earth & Environment*, 2(9), 645-658. https://doi.org/10.1038/s43017-021-00203-6

Ikuta, D., Ohtani, E., & Hirao, N. (2021). Two-phase mixture of iron–nickel–silicon alloys in the Earth's inner core. *Communications Earth & Environment*, 2(1), 1-10. https://doi.org/10.1038/s43247-021-00298-1

Khmelevska, T., Khmelevskyi, S., Ruban, A. V., & Mohn, P. (2006). Magnetism and origin of non-monotonous concentration dependence of the bulk modulus in Fe-rich alloys with Si, Ge and Sn: a first-principles study. *Journal of Physics: Condensed Matter*, *18*(29), 6677. https://doi.org/10.1088/0953-8984/18/29/009

Kohn, W., & Sham, L. J. (1965). Self-consistent equations including exchange and correlation effects. *Physical Review*, 140(4A), A1133. https://doi.org/10.1103/PhysRev.140.A1133

Kudrnovský, J., Christensen, N. E., & Andersen, O. K. (1991). Electronic structures and magnetic moments of $Fe_{3+y}Si_{1-y}$ and $Fe_{3-x}V_xSi$ alloys with DO_3-derived structure. *Physical Review B*, 43(7), 5924. https://doi.org/10.1103/PhysRevB.43.5924

Kulikov, N. I., Fristot, D., Hugel, J., & Postnikov, A. V. (2002). Interrelation between structural ordering and magnetic properties in bcc Fe-Si alloys. *Physical Review B*, *66*(1), 014206. https://doi.org/10.1103/PhysRevB.66.014206

Kádas, K., Vitos, L., Johansson, B., & Ahuja, R. (2009). Stability of body-centered cubic iron–magnesium alloys in the Earth's inner core. *Proceedings of the National Academy of Sciences*, 106(37), 15560-15562. https://doi.org/10.1073/pnas.0904859106

Mao, Z., Lin, J. F., Liu, J., Alatas, A., Gao, L., Zhao, J., & Mao, H. K. (2012). Sound velocities of Fe and Fe-Si alloy in the Earth's core. *Proceedings of the National*

Academy of Sciences, *109*(26), 10239-10244. https://doi.org/10.1073/pnas.1207086109

McDonough, W. F. (2003). 2.15–Compositional model for the Earth's core. *Treatise on geochemistry*, 2, 547-568. https://doi.org/10.1016/B0-08-043751-6/02015-6

Niu, Z. W., Zeng, Z. Y., Cai, L. C., & Chen, X. R. (2015). Study of the thermodynamic stability of iron at inner core from first-principles theory combined with lattice dynamics. *Physics of the Earth and Planetary Interiors*, 248, 12-19. https://doi.org/10.1016/j.pepi.2015.09.002

Ozawa, H., Hirose, K., Yonemitsu, K., & Ohishi, Y. (2016). High-pressure melting experiments on Fe–Si alloys and implications for silicon as a light element in the core. *Earth and Planetary Science Letters*, 456, 47-54. https://doi.org/10.1016/j.epsl.2016.08.042

Perdew, J. P., Burke, K., & Ernzerhof, M. (1996). Generalized gradient approximation made simple. *Physical Review Letters*, 77(18), 3865. https://doi.org/10.1063/1.472933

Ricolleau, A., Fei, Y., Corgne, A., Siebert, J., & Badro, J. (2011). Oxygen and silicon contents of Earth's core from high pressure metal–silicate partitioning experiments. *Earth and Planetary Science Letters*, *310*(3-4), 409-421. https://doi.org/10.1016/j.epsl.2011.08.004

Rinaldi, M., Mrovec, M., Fähnle, M., & Drautz, R. (2021). Determination of spin-wave stiffness in the Fe-Si system using first-principles calculations. *Physical Review B*, *104*(6), 064413. https://doi.org/10.1103/PhysRevB.104.064413

Sakai, T., Ohtani, E., Hirao, N., & Ohishi, Y. (2011). Stability field of the hcp-structure for Fe, Fe-Ni, and Fe-Ni-Si alloys up to 3 Mbar. *Geophysical Research Letters*, 38(9), L09302. https://doi.org/10.1029/2011GL047178

Sakamaki, T., Ohtani, E., Fukui, H., Kamada, S., Takahashi, S., Sakairi, T., Takahata, A., Sakai, T., Tsutsui, S., Ishikawa, D., Shiraishi, R., Seto, Y., Tsuchiya, T., & Baron, A. Q. (2016). Constraints on Earth's inner core composition inferred from measurements of the sound velocity of hcp-iron in extreme conditions. *Science Advances*, *2*(2), e1500802. https://doi.org/10.1126/sciadv.1500802

Sata, N., Hirose, K., Shen, G., Nakajima, Y., Ohishi, Y., & Hirao, N. (2010). Compression of FeSi, Fe_3C, $Fe_{0.95}O$, and FeS under the core pressures and implication for light element in the Earth's core. *Journal of Geophysical Research: Solid Earth*, 115(B9). https://doi.org/10.1029/2009JB006975

Shibazaki, Y., Nishida, K., Higo, Y., Igarashi, M., Tahara, M., Sakamaki, T., Terasaki, H., Shimoyama, Y., Kuwabara, S., Takubo, Y., & Ohtani, E. (2016).

Compressional and shear wave velocities for polycrystalline bcc-Fe up to 6.3 GPa and 800 K. *American Mineralogist*, *101*(5), 1150-1160. https://doi.org/10.2138/am-2016-5545

Shyni, P. C., & Alagarsamy, P. (2014). Thermomagnetic properties of nanocrystalline Fe–Si alloys with high Si content. *Physica B: Condensed Matter*, *448*, 60-63 https://doi.org/10.1016/j.physb.2014.02.032

Stixrude, L., & Cohen, R. E. (1995). High-pressure elasticity of iron and anisotropy of Earth's inner core. *Science*, 267(5206), 1972-1975. https://doi.org/10.1126/science.267.5206.1972

Tagawa, S., Gomi, H., Hirose, K., & Ohishi, Y. (2022). High‐temperature equation of state of FeH: Implications for hydrogen in Earth's inner core. *Geophysical Research Letters*, 49(5), e2021GL096260. https://doi.org/10.1029/2021GL096260

Tateno, S., Hirose, K., Ohishi, Y., & Tatsumi, Y. (2010). The structure of iron in Earth's inner core. *Science*, 330(6002), 359-361. https://doi.org/10.1126/science.1194662

Tateno, S., Kuwayama, Y., Hirose, K., & Ohishi, Y. (2015). The structure of Fe–Si alloy in Earth's inner core. *Earth and Planetary Science Letters*, *418*, 11-19. https://doi.org/10.1016/j.epsl.2015.02.008

Vočadlo, L., Alfè, D., Gillan, M. J., Wood, I. G., Brodholt, J. P., & Price, G. D. (2003). Possible thermal and chemical stabilization of body-centered-cubic iron in the Earth's core. *Nature*, 424(6948), 536-539. https://doi.org/10.1038/nature01829

References from the supporting information

Blanco, M. A., Francisco, E., & Luana, V. (2004). GIBBS: isothermal-isobaric thermodynamics of solids from energy curves using a quasi-harmonic Debye model. *Computer Physics Communications*, 158(1), 57-72. https://doi.org/10.1016/j.comphy.2003.12.001

Francisco, E., Recio, J. M., Blanco, M. A., Pendás, A. M., & Costales, A. (1998). Quantum-mechanical study of thermodynamic and bonding properties of MgF_2. *The Journal of Physical Chemistry A*, 102(9), 1595-1601. https://doi.org/10.1021/jp972516j

Momma, K., & Izumi, F. (2011). VESTA 3 for three-dimensional visualization of crystal, volumetric and morphology data. *Journal of applied crystallography*, 44(6), 1272-1276. https://doi.org/10.1107/S0021889811038970

Moruzzi, V. L., Janak, J. F., & Schwarz, K. (1988). Calculated thermal properties of metals. *Physical Review B*, 37(2), 790. https://doi.org/10.1103/PhysRevB.37.790

415

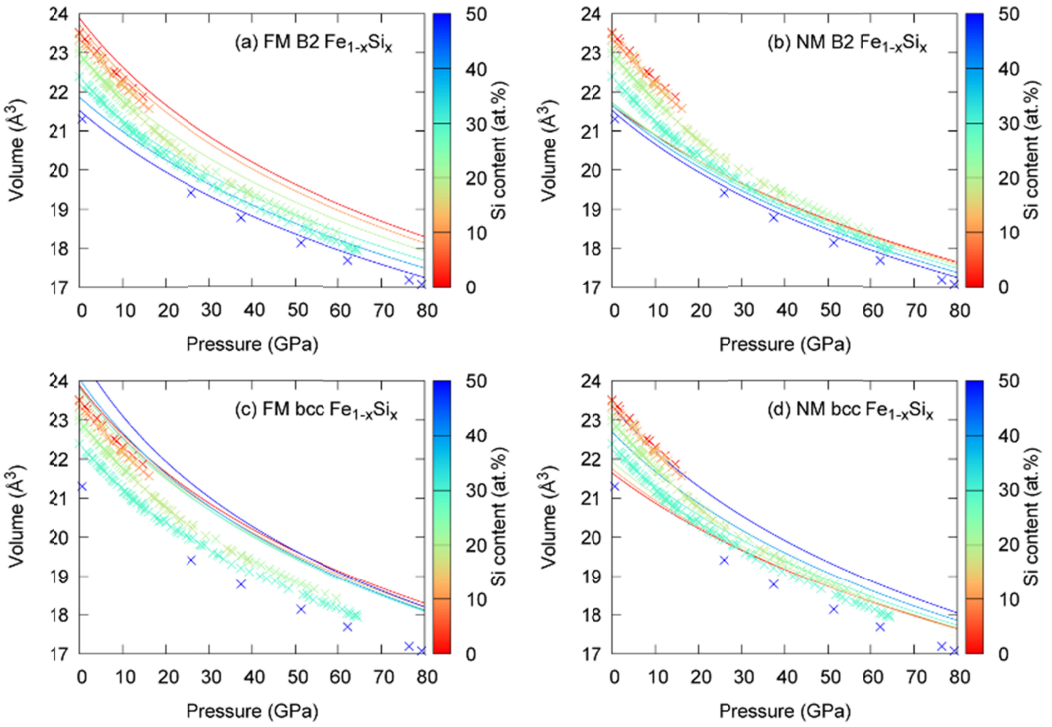

417

421 **Figure 1.** Present equations of state for: (a) ferromagnetic (FM) B2, (b) non-magnetic
422 (NM) B2, (c) FM bcc, and (d) NM bcc $Fe_{1-x}Si_x$. The solid lines indicate the present
423 calculations, and the cross symbols correspond to previous experiments for B2 and bcc
424 $Fe_{1-x}Si_x$ (Dewaele et al., 2006; Edmund et al., 2019; Sata et al., 2010).

422

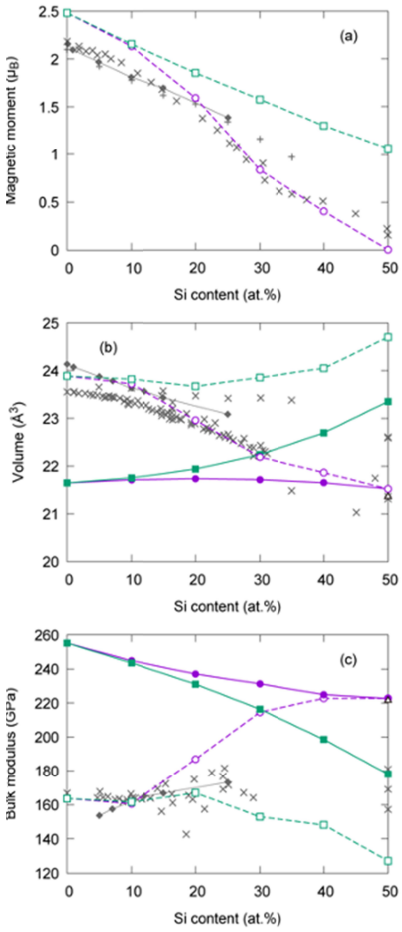

423

432 **Figure 2.** (a) The bulk magnetic moment of ferromagnetic (FM) B2 (purple circles)
433 and bcc (green squares) $Fe_{1-x}Si_x$ at 0 GPa. Earlier theoretical (♦, Kulikov et al., 2002)
434 and experimental (+, Shyni and Alagarsamy, 2014; ×, Elsukov et al., 1992 and
435 references therein) studies are also plotted. (b) Ambient pressure volume of FM B2
436 (open purple circles), non-magnetic (NM) B2 (filled purple circles), FM bcc (open
437 green squares), and NM bcc (filled green squares) $Fe_{1-x}Si_x$. Previous theoretical (♦,
438 Kulikov et al., 2002) and experimental (△, Sata et al., 2010; ×, Edmund et al., 2019
439 and references therein) data is shown for comparison. (c) Zero-pressure bulk modulus.
440 The symbols are the same as those for the volume.

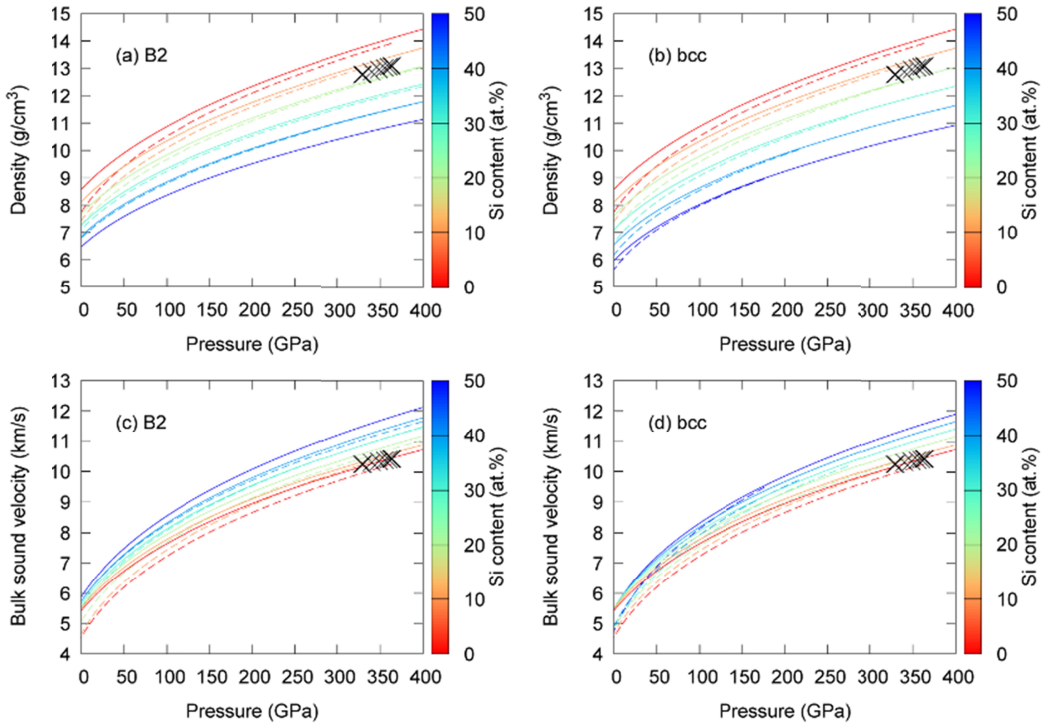

433

438 **Figure 3.** The density and bulk sound velocity as a function of pressure. Trends for B2

439 $Fe_{1-x}Si_x$ (a, c) and bcc $Fe_{1-x}Si_x$ (b, d) with x = 0 (red), 0.1, 0.2, 0.3, 0.4, and 0.5 (blue).

440 Solid and broken lines indicate ferromagnetic (FM) and non-magnetic (NM) states,

441 respectively. The cross symbols indicate the PREM values at the inner core

442 (Dziewonski and Anderson, 1981).

439

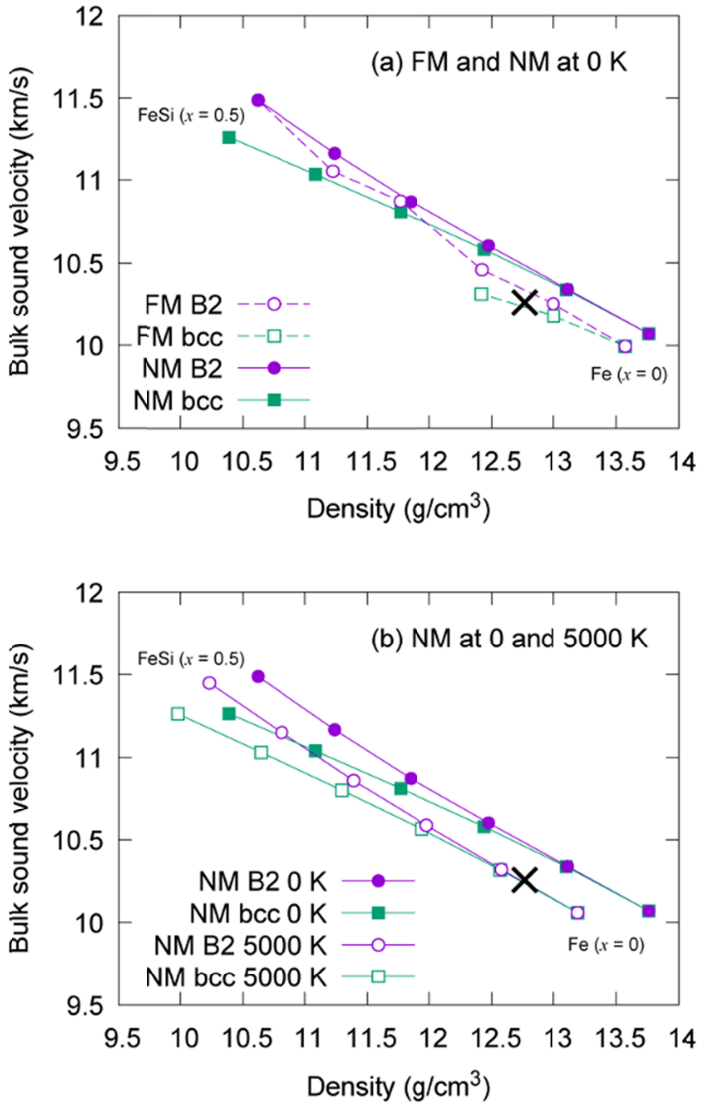

440

444 **Figure 4.** (a) The density and bulk sound velocity of B2 and bcc $Fe_{1-x}Si_x$ alloys at the
445 ICB pressure and 0 K. (b) The density and bulk sound velocity of B2 and bcc $Fe_{1-x}Si_x$
446 alloys at the ICB pressure and both 0 and 5000 K; the PREM value is plotted as cross
447 symbol for comparison (Dziewonski and Anderson, 1981).

445

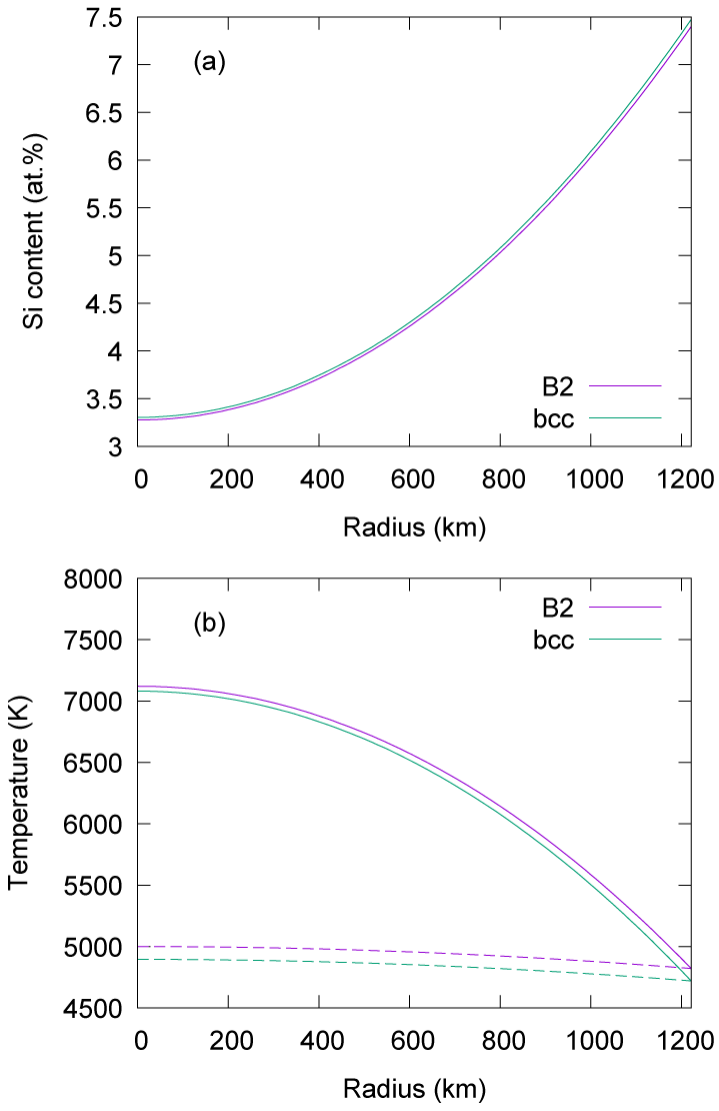

445

446 **Figure 5.** (a) The Si content and (b) temperature profiles that simultaneously satisfy
447 the density and bulk sound velocity of the PREM inner core (Dziewonski and
448 Anderson, 1981). Note that the calculated temperature gradients (solid lines) are
449 steeper than the adiabatic temperature gradients (broken lines), implying that bcc-like
450 $Fe_{1-x}Si_x$ alone cannot explain the PREM (Dziewonski and Anderson, 1981).